SAFETY FACTOR ANALYSIS OF NATURAL SLOPES USING RIGID PLASTIC FINITE ELEMENT METHOD (RPFEM)

Pham Ngoc Quang*, Pham Ngoc Vinh

The University of Danang - University of Science and Technology, Vietnam

*Corresponding author: pnquang@dut.udn.vn

(Received: October 01, 2024; Revised: October 25, 2024; Accepted: November 14, 2024)

DOI: 10.31130/ud-jst.2024.428E

Abstract - In this study, a new method for analyzing safety factor (F_s) of natural slopes was developed. Rigid-plastic constitutive equation for soil materials and a slope stability analysis framework were formulated to account for both soil properties (cohesive strength c and friction angle ϕ) and slope geometry (slope angle β and slope height H). These models enable the analysis of cohesive and frictional strengths within slopes while avoiding the need for excessive element subdivision, thereby allowing for high-precision analysis. To demonstrate the effectiveness of the developed model, its validity was first verified through numerical analysis of simple models with known solutions. The results indicate that this method can reasonably evaluate the stability of slopes across a wide range of soil properties and geometric conditions.

Key words – Safety factor; Cohesive strength; Frictional strength; Slope angle; Slope height; RPFEM.

1. Introduction

In natural slopes, the presence of weak soil layers, particularly in relation to soil properties such as cohesion, internal friction angle, and unit weight, often plays a critical role in initiating slope failures. These weak layers typically exhibit lower shear strength compared to the surrounding soil, making them more susceptible to failure under stress conditions. The failure mode of the slope is predominantly governed by these localized weak layers, as they act as planes of weakness where slip surfaces are likely to form. Without taking these weak layers into account during analysis, it is impossible to accurately predict or represent the complex mechanisms involved in slope failure.

In the case of landslides, once a slip surface is clearly formed within the slope, it is often found that the weak layer propagates along this surface, further reducing the safety factor and exacerbating instability. The occurrence of thin weak layers within slopes is not uncommon and can significantly influence both the initiation and progression of failure, directly impacting the overall safety factor [1 - 8]. These weak layers alter the stress distribution and deformation behavior of the slope, leading to a failure mechanism that is vastly different from what would occur in homogeneous soil conditions. Consequently, the evaluation of the safety factor, particularly with the inclusion of weak layers, becomes a critical aspect of slope stability analysis in geotechnical engineering. Accurately modeling and understanding the behavior of these weak layers under various loading conditions is crucial for predicting potential failures and calculating reliable safety factors. By incorporating these considerations, engineers can develop more accurate models and design approaches that ensure the long-term stability and safety of slopes in natural environments.

This study focuses on slope stability analysis by calculating the safety factor using the Rigid Plastic Finite Element Method (RPFEM). The rigid plastic constitutive model, developed from the upper bound theorem of limit analysis, defines a relationship based on the governing equations. In geotechnical engineering, Tamura et al. [9-11] introduced the methodology for deriving this model. Following Tamura's approach, the rigid plastic model in this study incorporates shear strength reduction and penalty methods, essential for evaluating the safety factor of slopes. The accuracy of the method is validated through numerical analysis of a simple model with a known solution. An in-house RPFEM code developed by the author [12-25] is used to compute the safety factor of the natural slope. The RPFEM has proven effective in geotechnical engineering applications, as demonstrated in previous works [26-34], further supporting its reliability in calculating safety factors and enhancing slope stability analysis.

The applicability of the developed constitutive model will be assessed by evaluating the safety factor of natural slopes, considering key factors like soil properties (cohesion c and friction angle ϕ) and slope geometry (slope angle β and height H). It is anticipated that the safety factor will exhibit significant variability depending on these parameters, with the interaction between cohesion and friction playing a crucial role that is influenced by both the slope angle and the slope height. This study aims to demonstrate the effectiveness of the proposed method in accurately evaluating slope stability, thereby contributing to improved engineering practices and more reliable safety factor assessments for slopes in various geotechnical contexts and applications.

2. Methodology for slope stability analysis

2.1. Rigid plastic constitutive equation for soil materials

Tamura et al. [9 - 11] derived a rigid-plastic constitutive equation using a yield function of the type. The yield function is expressed using the first invariant of the stress tensor $I_1 = tr(\boldsymbol{\sigma})$ and the second invariant of the deviatoric stress tensor $J_2 = \frac{1}{2}\mathbf{s}:\mathbf{s}$ as follows. Here, $a = \frac{\tan\phi}{\sqrt{9+12\tan^2\phi}}$ and $b = \frac{3c}{\sqrt{9+12\tan^2\phi}}$ are coefficients

related to cohesive strength c and frictional strength ϕ of soil based on the Mohr-Coulomb failure criterion. Defining tensile stress as positive, and representing the stress tensor as **σ**, and the deviatoric stress tensor as **s**, the equation becomes the following.

$$f(\boldsymbol{\sigma}) = aI_1 + J_2 - b = 0 \tag{1}$$

The stress **σ** is decomposed into the determinable stress $\boldsymbol{\sigma}_{(1)}$, which can be obtained from the plastic strain rate, and the indeterminable stress $\boldsymbol{\sigma}_{(2)}$, which cannot be derived from the plastic strain rate. The determinable stress $\boldsymbol{\sigma}_{(1)}$ is expressed as follows according to the associated flow rule.

$$\boldsymbol{\sigma}_{(1)} = \frac{b}{\sqrt{3a^2 + 0.5}} \frac{\dot{\boldsymbol{\varepsilon}}^p}{\dot{e}} \text{ with } \dot{e} = \sqrt{\dot{\boldsymbol{\varepsilon}}^p : \dot{\boldsymbol{\varepsilon}}^p} \tag{2}$$

in which, $\dot{e}$ represents the plastic strain rate, and $\dot{\boldsymbol{\varepsilon}}^p$ represents the equivalent plastic strain rate. The indeterminable stress $\boldsymbol{\sigma}_{(2)}$ is the stress component that lies along the linear portion of the yield function expressed in Eq. (1) and cannot be directly obtained from the constitutive equation. However, by utilizing the presence of stress on the yield function, the components of the indeterminable stress can be expressed as follows:

$$h(\dot{\boldsymbol{\varepsilon}}^p) = \dot{\varepsilon}_v^p - \frac{3a}{\sqrt{3a^2 + 0.5}} \dot{e} = \dot{\varepsilon}_v^p - \eta \dot{e} = 0 \tag{3}$$

Here, $\dot{\varepsilon}_v^p$ represents the plastic volumetric strain rate. Using the fact that Eq. (3) represents the plastic strain rate being orthogonal to the yield function in Eq. (1), the indeterminate stress $\boldsymbol{\sigma}_{(2)}$ can be expressed with an unknown coefficient λ, which remains undetermined until the boundary value problem in Eq. (3) is solved.

$$\boldsymbol{\sigma}_{(2)} = \lambda \frac{\partial h}{\partial \dot{\boldsymbol{\varepsilon}}^p} = \lambda \left(\mathbf{I} - \frac{3a}{\sqrt{3a^2 + 0.5}} \frac{\dot{\boldsymbol{\varepsilon}}^p}{\dot{e}} \right) \tag{4}$$

in which, ***I*** shows the unit tensor. From Eq. (2) and Eq. (4), the rigid-plastic constitutive equation for the Druker-Prager type yield function (shown in Figure 1), is given by the following equation.

$$\boldsymbol{\sigma} = \boldsymbol{\sigma}_{(1)} + \boldsymbol{\sigma}_{(2)} = \frac{b - 3a\lambda}{\sqrt{3a^2 + 0.5}} \frac{\dot{\boldsymbol{\varepsilon}}^p}{\dot{e}} + \lambda \mathbf{I} \tag{5}$$

Although this constitutive equation includes the undetermined coefficient λ, it can be determined by analyzing the boundary value problem together with the constraint conditions of Eq. (3).

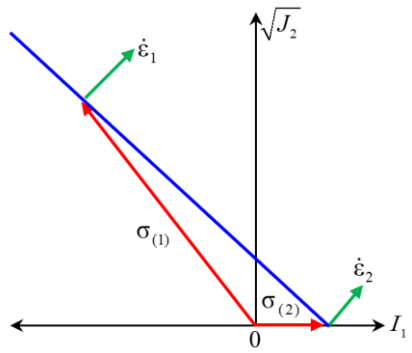

Figure 1. *Drucker-Prager yield function [24, 31]*

2.2. Rigid plastic constitutive equation for slope stability analysis

In slope stability analysis, by convention, the safety factor F_s of the slope is defined by the reduction rate of the soil strength. In slope stability analysis, under certain load conditions (such as surface loads or body forces), the ultimate state of the slope is produced by altering the shear strength of the soil using a strength reduction factor, and the safety factor is then determined. Therefore, even in slopes with a safety factor greater than F_s>1.0, a hypothetical failure mode can be obtained as the analysis result by applying the operation of reducing the soil strength according to the safety factor. The yield functions in Eqs. (1) and (3), along with the volume change characteristics, are expressed in the following equation using the strength reduction factor [31].

$$f(\boldsymbol{\sigma}, F_s) = \frac{a}{F_s} I_1 + J_2 - \frac{b}{F_s} = \hat{a} I_1 + J_2 - \hat{b} = 0 \tag{6}$$

$$h(\dot{\boldsymbol{\varepsilon}}^p, F_s) = \dot{\varepsilon}_v^p - \frac{3\hat{a}}{\sqrt{3\hat{a}^2 + 0.5}} \dot{e} = \dot{\varepsilon}_v^p - \hat{\eta} \dot{e} = 0 \tag{7}$$

Here, $\hat{\eta}$ is the coefficient obtained from Eq. (7) when using the strength reduction factor.

In addition, in this study, to accelerate the analysis speed, the constraint conditions are explicitly addressed using the penalty method (κ: penalty constant). Based on the above, the rigid-plastic constitutive equation is ultimately given by the following equation.

$$\boldsymbol{\sigma} = \frac{\hat{b}}{\sqrt{3\hat{a}^2 + 0.5}} \frac{\dot{\boldsymbol{\varepsilon}}^p}{\dot{e}} + \kappa \left(\dot{\varepsilon}_v^p - \hat{\eta} \dot{e} \right) \left(\mathbf{I} - \frac{3\hat{a}}{\sqrt{3\hat{a}^2 + 0.5}} \frac{\dot{\boldsymbol{\varepsilon}}^p}{\dot{e}} \right) \tag{8}$$

Slope stability analysis is conducted by substituting the rigid-plastic constitutive equation from Eq. (8) into the force balance equation (weak form). Here, the body forces are represented by **x** (where V is the analysis domain) and the surface forces by **t** (where S_σ is the stress boundary), leading to the following expression after some expansion.

$$\int_V \left(\frac{b - 3a\kappa\left(\dot{\varepsilon}_v^p - \hat{\eta}\dot{e}\right)}{\sqrt{3\hat{a}^2 + 0.5}} \frac{\dot{\boldsymbol{\varepsilon}}^p}{\dot{e}} \right) : \delta\dot{\boldsymbol{\varepsilon}}^p dV + \int_V \left(F_s \cdot \kappa \right) \left(\dot{\varepsilon}_v^p - \hat{\eta}\dot{e} \right) \mathbf{I} : \delta\dot{\boldsymbol{\varepsilon}}^p dV = \int_V \left(F_s \cdot \mathbf{x} \right) \cdot \delta\dot{\mathbf{u}} dV + \int_{S_\sigma} \left(F_s \cdot \mathbf{t} \right) \cdot \delta\dot{\mathbf{u}} dS \tag{9}$$

for $\forall \delta\dot{\mathbf{u}}$.

Due to the indeterminacy of the magnitude of the displacement rate in the rigid-plastic constitutive equation, the strength reduction factor (safety factor) can be determined by analyzing it along with the following constraint conditions.

$$\int_V \mathbf{x} \cdot \dot{\mathbf{u}} dV + \int_{S_\sigma} \mathbf{t} \cdot \dot{\mathbf{u}} dS = 1 \tag{10}$$

In slope stability analysis, as indicated in Eqs. (6) and (7), the strength parameters and volume change characteristics of the soil vary according to the strength reduction factor, making Eq. (8) a nonlinear equation concerning the strength reduction factor. Therefore, by assuming the strength reduction factor Fs and the initial

displacement rate $\dot{\mathbf{u}}$, Eq. (9) can be solved to calculate and update both the strength reduction factor and the displacement rate using an iterative method. By explicitly incorporating the constraint condition Eq. (10) into Eq. (9) using the penalty method (μ: penalty constant), the following expression is obtained.

$$\int_V \left(\frac{b - 3a\kappa\left(\dot{\varepsilon}_v^p - \hat{\eta}\dot{e}\right)}{\sqrt{3\hat{a}^2 + 0.5}} \frac{\dot{\boldsymbol{\varepsilon}}^p}{\dot{e}} \right) : \delta\dot{\boldsymbol{\varepsilon}}^p dV + \int_V \left(F_s \cdot \kappa\right)\left(\dot{\varepsilon}_v^p - \hat{\eta}\dot{e}\right)\mathbf{I} : \delta\dot{\boldsymbol{\varepsilon}}^p dV$$
$$= \mu\left(\int_V \mathbf{x}\cdot\dot{\mathbf{u}}dV + \int_{S_\sigma} \mathbf{t}\cdot\dot{\mathbf{u}}dS - 1\right)\int_V \mathbf{x}\cdot\delta\dot{\mathbf{u}}dV + \int_{S_\sigma} \mathbf{t}\cdot\delta\dot{\mathbf{u}}dS \tag{11}$$

When the displacement rate $\dot{\mathbf{u}}$ is determined from the analysis of Eq. (11), the strength reduction factor can be obtained from the following equation, allowing the safety factor to be calculated.

$$F_s = \mu\left(\int_V \mathbf{x}\cdot\dot{\mathbf{u}}dV + \int_{S_\sigma} \mathbf{t}\cdot\dot{\mathbf{u}}dS - 1\right) \tag{12}$$

3. Numerical simulation considering factors related to slope failure

3.1. Effect of soil shear strengths (c and ϕ) on safety factor F_s

This study investigates the effect of soil shear strengths (cohesive strength *c* and frictional strength ϕ) on slope stability. A slope model shown in Figure 2, was adopted for the numerical simulation. The bottom boundary is set as a fixed condition, and the side boundaries are set as roller conditions (restrained in one direction only). Table 1 presents the shear strength parameters. The geometry of the natural slope is presented in Figure 1. Three slope angles were considered β=15°, 30°, and 45°. Several slope heights *H* were used in the range of 5.0 m – 25.0 m, in Table 2.

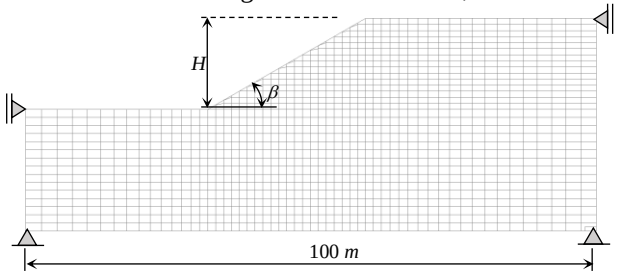

Figure 2. *Boundary condition of natural slope model using rigid plastic finite element method (RPFEM)*

Table 1. *Parameters for soil shear strengths (c, and ϕ)*

Shear strength *c* (kPa)	Frictional strength *ϕ* (deg)	Soil unit weight γ (kN/m^3)
1 - 30	30, 35, and 40	18.0

Table 2. *Parameters for slope geometry (β, and H)*

Slope angle *β* (°)	Slope height *H* (m)
15 °, 30 °, and 45°	5 m, 15 m, and 25 m

Figure 3 presents the relationship between cohesive strength (*c*) and safety factor F_s, demonstrating that the safety factor increases as frictional strength ϕ rises. This is a key observation in slope stability analysis, as it indicates that slopes with higher frictional strength are more stable and have a reduced risk of failure. The frictional strength reflects the ability of soil to resist sliding, so an increase in this parameter results in greater stability under load.

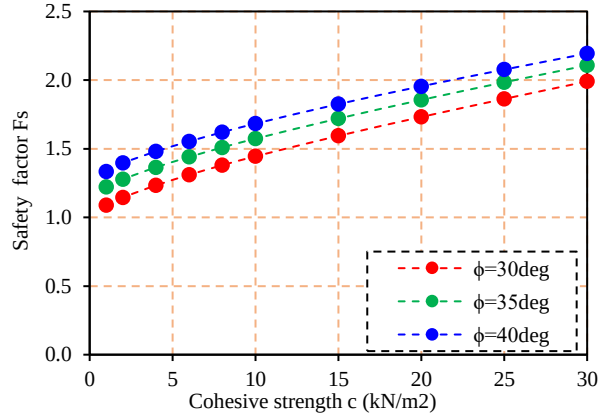

Figure 3. *Effect of soil shear strengths (c and ϕ) on safety factor F_s of a natural slope considering slope of β=30°, and H=15 m*

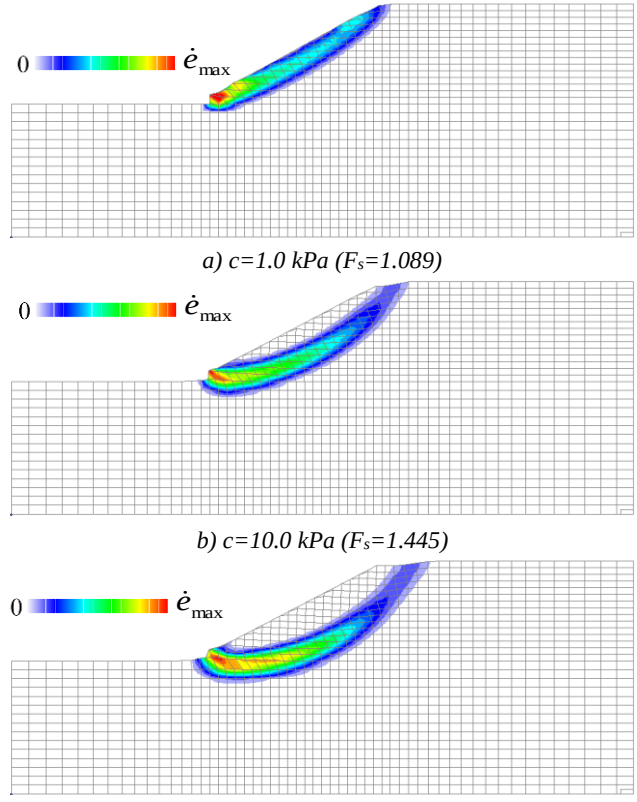

a) c=1.0 kPa (F_s=1.089)

b) c=10.0 kPa (F_s=1.445)

c) *c*=30.0 kPa (F_s=1.990)

Figure 4. *Strain rate distribution of a natural slope for varying cohesion values (c) with a friction angle of ϕ=30°, at a slope angle of β=30° and a height of H=15 m*

Additionally, Figure 4 presents the strain rate distributions for various cases, effectively illustrating how different levels of cohesion *c* influence deformation and failure patterns in slopes. In scenarios with low cohesion *c*, the slope is prone to surface failure, indicating that the uppermost layers are more susceptible to sliding. This type of shallow failure is commonly linked to weaker soil conditions, where insufficient cohesive strength *c* heightens the slope's vulnerability to erosion and surface sliding, particularly during external loading or

environmental changes, such as rainfall. Conversely, as cohesion c increases, the failure mechanism transitions from shallow to deeper layers of the slope. The failure surface, which delineates the sliding mass, shifts inward and downward, leading to deep-seated failure. This mechanism involves larger volumes of soil and occurs deeper within the slope, driven by the enhanced cohesive forces present in the soil. The increased cohesion enables the upper layers to remain stable, yet it also concentrates strain in the deeper layers, resulting in a more complex and profound failure mechanism. These findings align remarkably well with those of Hoshina et al. [31], reinforcing the validity of the proposed models.

This observation is crucial because it demonstrates that varying levels of cohesive strength c can result in distinctly different failure modes. In low-cohesion soils, shallow failures are more likely, while higher-cohesion soils tend to experience deeper failures. Understanding these differences is essential for engineers and geotechnical experts when designing slope stabilization measures or predicting the potential failure mode of a slope. By considering the cohesion and frictional strength of the soil, appropriate reinforcement strategies, such as slope reinforcement or drainage systems, can be implemented to mitigate the risk of both shallow and deep-seated failures.

3.2. Effect of slope angle β on safety factor F_s

To verify the effect of slope angle, Figure 5 illustrates the relationship between slope angle (β) and the safety factor (F_s) for different values of cohesive strength (c). The analysis reveals a clear inverse correlation: as the slope angle increases, the safety factor consistently decreases. This reduction in Fs is particularly significant when β rises from 15° to 45°, indicating heightened instability. As the slope angle increases, the driving forces acting on the slope intensify, while the resisting forces governed by soil cohesion and internal friction become less effective. Consequently, the slope's ability to withstand external loads diminishes, leading to a more pronounced decline in safety factor. These findings align with those of Hoshina et al. [31], emphasizing the importance of considering slope angle in stability assessments.

Figure 6 illustrates the failure modes of a natural slope across a range of slope angles (β = 15° to 45°). It is evident that the failure surface extends from the crest of the slope down to the toe, indicating a progressive failure mechanism. When comparing the failure modes at a small slope angle (β = 15°) to those at a steeper angle (β = 45°), it becomes clear that the failure surface is more localized near the crest in the case of the steeper slope. This can be attributed to the increased influence of soil weight, which acts as an additional destabilizing force. The gravitational load intensifies the driving forces, contributing to the overall instability of the slope.

The numerical results obtained from the Rigid Plastic Finite Element Method (RPFEM) further confirm this trend. At a slope angle of β = 15°, the safety factor (F_s) was calculated to be approximately F_s=2.455, indicating relatively stable conditions. However, as the slope angle increased to β=45°, the safety factor dropped significantly to F_s=1.083, suggesting a much higher risk of failure. As β continues to increase beyond β=45°, the slope ultimately experiences a full-scale failure, driven predominantly by gravitational forces. This overall failure mode highlights the critical role of slope angle in the stability of natural slopes, where steeper angles lead to the concentration of failure mechanisms near the crest, and the weight of the soil accelerates the progression towards instability.

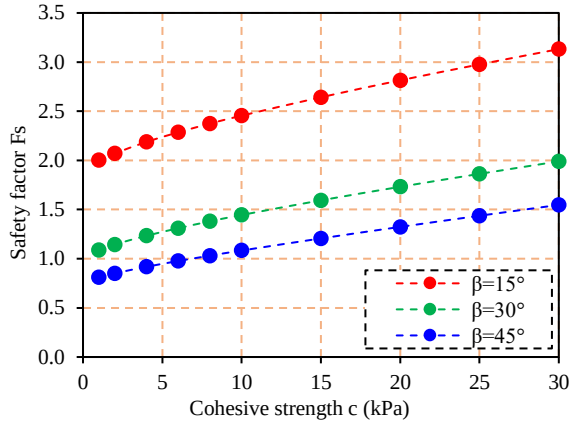

Figure 5. *Effect of slope angle β on safety factor F_s of a natural slope considering slope of ϕ=30deg, and H=15.0 m*

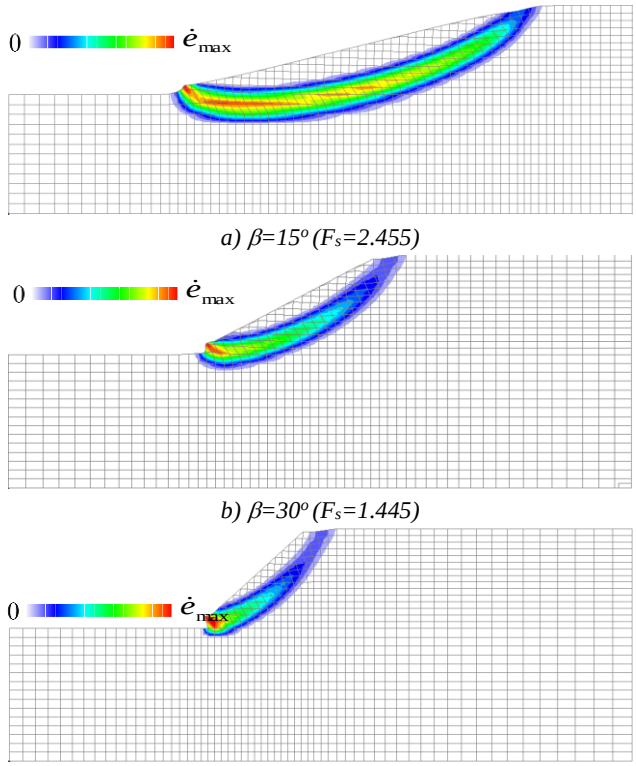

a) β=15° (F_s=2.455)

b) β=30° (F_s=1.445)

c) β=45° (F_s=1.083)

Figure 6. *Strain rate distribution of a natural slope for various slope angles (β) with H=15 m, considering ϕ=30° and c=10 kPa*

3.3. Effect of slope height H on safety factor F_s

To verify the effect of slope height (H), a series of analyses was conducted with heights ranging from H=5 m to H=25 m. Figure 7 shows the relationship between the safety factor (F_s) and the cohesive strength (c) for a typical case where the internal friction angle is ϕ=30° and the slope angle is β=30°. The results indicate that F_s decreases as H

increases due to the added weight of the soil mass, which raises the driving forces that can cause slope failure. As the slope height increases, the destabilizing forces grow, reducing overall stability. Consequently, taller slopes are more prone to instability, especially when soil strength remains constant, in agreement with Hoshina et al. [31].

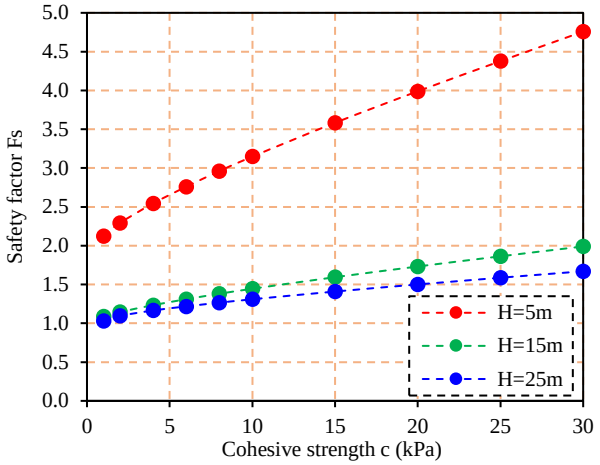

Figure 7. *Effect of slope height (H) on safety factor (F_s) for a slope with a friction angle of ϕ=30° and a slope angle of β=30°*

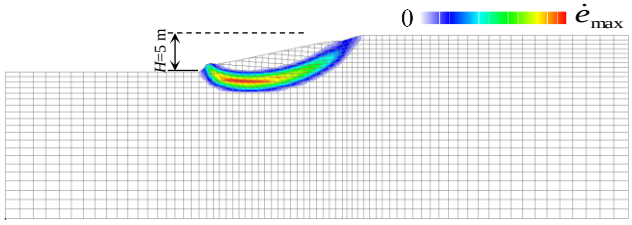

a) H=5 m (F_s=3.584)

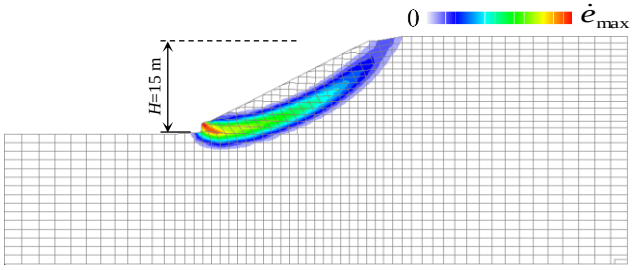

b) H=15 m (F_s=1.445)

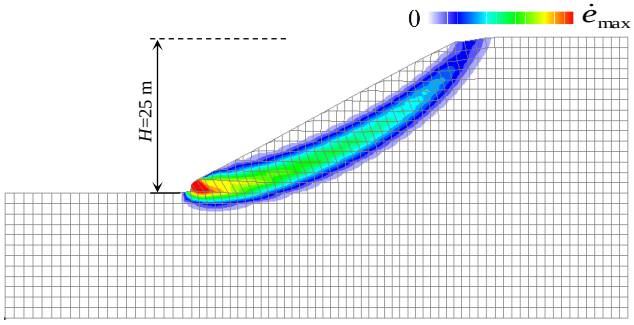

c) H=25 m (F_s=1.309)

Figure 8. *Strain rate distribution of a natural slope for varying heights (H) at a slope angle of β = 30°, considering a friction angle of ϕ=30° and a cohesion of c=10 kPa*

Additionally, Figure 8 presents the failure modes of the natural slope for three cases: H=5 m, 15 m, and 25 m. It can be observed that the failure areas of the natural slope expand as the slope height H increases. However, the safety factor decreases from approximately F_s=3.584 for H=5 m to F_s=1.309 for H=25 m. The increase in the failure area and the decrease in the safety factor are due to the greater mass of soil involved in the failure mechanism as slope height increases. Taller slopes generate larger gravitational forces acting on the soil, which increases the likelihood of movement and instability. Consequently, the stability of the slope diminishes with increasing height, leading to a significant reduction in the safety factor. In summary, as slope height (H) increases, both the failure area and the risk of slope failure increase, as reflected by the corresponding reduction in the safety factor.

The relationship between slope height and slope stability is critical. As the height of a slope increases, the added weight of the soil mass results in greater driving forces that can lead to failure. At the same time, the resisting forces may become insufficient to counterbalance the increased load. Therefore, taller slopes are inherently more susceptible to instability, especially when the soil's shear strength remains constant. This underscores the importance of carefully considering slope height in geotechnical engineering and implementing effective measures, such as reinforcement or drainage systems, to ensure slope stability.

4. Conclusions

The key conclusions derived from the study are as follows:

(1) The derived rigid-plastic constitutive equations and the proposed stability analysis method significantly enhance the understanding of slope behavior under various conditions. This method reliably assesses slope stability and provides valuable insights for geotechnical engineering applications.

(2) The study demonstrates that higher frictional strength (ϕ) increases slope stability by raising the safety factor (F_s), while greater cohesion (c) shifts failure mechanisms from shallow surface failures to deeper-seated failures. Improved cohesion keeps the upper layers intact, but redistributes strain deeper, leading to more complex failure modes involving larger soil volumes. This underscores the critical role of cohesive strength in slope stability and failure behavior.

(3) Slope angle (β) significantly affects slope stability, with steeper angles leading to a lower safety factor and a heightened risk of failure. This occurs because increased slope angles amplify gravitational driving forces while diminishing the effectiveness of resisting forces. Therefore, careful consideration of slope angle is essential in geotechnical design to ensure stability.

(4) Increasing slope height (H) markedly decreases slope stability due to enhanced gravitational forces that elevate the risk of failure. This results in a significant reduction in the safety factor (F_s) and larger failure areas. Therefore, it is crucial to consider slope height in geotechnical design and implement effective stabilization measures to mitigate potential instability.

Acknowledgment: PHAM Ngoc Quang received a Postdoctoral Scholarship with code VINIF.2023.STS.12 from the Vingroup Innovation Foundation (VINIF).

REFERENCES

[1] S. Ohtsuka and Y. Miyata. "Slope stability analysis taking into account pre-existing slip lines", In *Proc. of 10th International Conference on International Association for Computer Methods and Advances in Geomechanics*, vol. 2, pp. 1601-1604, 2001.

[2] C. Fei, U. Keizo, and H. Wenfeng. "Slope stability analysis: Comparisons between limit equilibrium methods and elastoplastic finite element method", *Landslides*, vol. 39, no. 4, pp. 395-402, 2003.

[3] E. Yusuf and T. Cetin. "The prediction of the critical factor of safety of homogeneous finite slopes using neural networks and multiple regressions", *Computers & Geosciences*, vol. 51, pp. 305-313, 2013.

[4] F. Xianda, S. Li, C. Yuan, P. Zeng, and Y. Sun. "Prediction of slope stability using naive Bayes classifier", *KSCE Journal of Civil Engineering*, vol. 22, pp. 941-950, 2018.

[5] S. Rukhaiyar, M. N. Alam, and N. K. Samadhiya. "A PSO-ANN hybrid model for predicting factor of safety of slope", *International Journal of Geotechnical Engineering*, vol. 12, no. 6, pp. 556-566, 2018.

[6] S. Farzin and F. Jafari. "A simple direct method for prediction of safety factor of homogeneous finite slopes", *Geotechnical and Geological Engineering*, vol. 37, no. 5, pp. 3949-3959, 2019.

[7] M. Balendra, A. Kukunuri, and R. S. Jakka. "Improvement in prediction of slope stability & relative importance factors using ANN", *Geotechnical and Geological Engineering*, vol. 39, no. 8, pp. 5879-5894, 2021.

[8] M. Arsalan, M. Mohammadi, H. F. H. Ali, H. H. Ibrahim, S. N. Abdulhamid, and H. R. Nejati. "*Prediction of safety factors for slope stability: comparison of machine learning techniques*", Natural Hazards, 2022, pp. 1-29.

[9] T. Tamura, S. Kobayashi, and T. Sumi, "Limit analysis of soil structure by rigid plastic finite element method", *Soils and Foundations*, vol. 24, no. 1, pp.34-42, 1984.

[10] T. Tamura, S. Kobayashi, and T. Sumi, "Rigid-plastic finite element method for frictional materials", *Soils and Foundations*, vol. 27, no. 3, pp. 1-12, 1987.

[11] T. Tamura, "Rigid-plastic finite element method in geotechnical engineering", In *Computational Plasticity*. 1990.

[12] P. N. Quang, S. Ohtsuka, K. Isobe, and Y. Fukumoto. "*Effect of Ground Movement Direction on Ultimate Lateral Resistance of Line Alignment Piles in Clay",* GIGAKU, 2018.

[13] P. N. Quang, S. Ohtsuka, K. Isobe, and Y. Fukumoto. "Group effect on ultimate lateral resistance of piles against uniform ground movement", *Soils and Foundations*, vol. 59, no. 1, pp. 27-40, 2019.

[14] P. N. Quang, S. Ohtsuka, K. Isobe, Y. Fukumoto, and T. Hoshina, "Ultimate bearing capacity of rigid footing under eccentric vertical load", *Soils and Foundations*, vol. 59, no. 6, pp. 1980-1991, 2019.

[15] P. N. Quang, S. Ohtsuka, K. Isobe, and Y. Fukumoto, "Limit load space of rigid footing under eccentrically inclined load", *Soils and Foundations*, vol. 60, no. 4, pp. 811-824, 2020.

[16] P. N. Quang. "*Estimation of Ultimate Lateral Resistance of Pile Group, and Ultimate Bearing Capacity of Rigid Footing under Complex Load by using Rigid Plastic Finite Element Method*", (Doctoral dissertation, Nagaoka University of Technology), 2020.

[17] P. N. Quang and S. Ohtsuka, "Ultimate bearing capacity of rigid footing on two-layered soils of sand–clay", *International Journal of Geomechanics*, vol. 21, no. 7, p.04021115, 2021.

[18] P. N. Quang, S. Ohtsuka, K. Isobe, and Y. Fukumoto, "Consideration on Limit Load Space of Footing on Various Soils Under Eccentric Vertical Load", In *Challenges and Innovations in Geomechanics: Proceedings of the 16th International Conference of IACMAG*, vol. 2, no. 16, pp. 75-84, 2021.

[19] P. N. Quang, S. Ohtsuka, K. Isobe, and Y. Fukumoto, "Limit load space of rigid strip footing on cohesive-frictional soil subjected to eccentrically inclined loads", *Computers and Geotechnics*, vol. 151, pp. 104956, 2022.

[20] P. N. Quang and S. Ohtsuka, "Numerical Investigation on Bearing Capacity of Rigid Footing on Sandy Soils Under Eccentrically Inclined Load", In *Proceedings of the 2nd Vietnam Symposium on Advances in Offshore Engineering: Sustainable Energy and Marine Planning*. Springer Singapore, 2022, pp. 333-341.

[21] P. N. Quang, S. Ohtsuka, K. Isobe, N.V. Pham, and P.H. Hoang, "Limit load space of rigid strip footing on sand slope subjected to combined eccentric and inclined loading", *Computers and Geotechnics*, vol. 162, pp. 105652, 2023.

[22] P. N. Quang, S. Ohtsuka, K. Isobe, and P.H. Hoang, "Ultimate bearing capacity of rigid strip footings on c-ϕ soil subjected to combined eccentric and inclined loading", *in IOP Conference Series: Materials Science and Engineering*, vol. 1289, no. 1, p. 012088. IOP Publishing, 2023.

[23] P. N. Vinh, P. N. Quang, and H. Thang, "Effect of foundation surface roughness on ultimate bearing capacity of an eccentrically loaded foundation", *the University of Danang – Journal of Science and Technology*, vol. 21, no. 12.1, pp. 28–33, 2023.

[24] P. N. Quang and P. N. Vinh, "Effect of footing roughness on ultimate bearing capacity of rigid strip footing on sandy soil slope", *the University of Danang – Journal of Science and Technology*, vol. 21, no. 12.1, pp. 22–27, 2023.

[25] P. N. Quang and P. N. Vinh, "Estimation of ultimate bearing capacity of strip footings on cohesive-frictional soils using non-linear shear strength model", *the University of Danang – Journal of Science and Technology*, vol. 22, no. 6.A, pp. 29–34, 2024.

[26] F. Tatsuoka, M. Sakamoto, T. Kawamura, and S. Fukushima, "Strength and deformation characteristics of sand in plane strain compression at extremely low pressures", *Soils and Foundations*, vol 26, no. 1, pp. 65-84, 1986.

[27] A. Asaoka and S. Ohtsuka, "The analysis of failure of a normally consolidated clay foundation under embankment loading", *Soils and Foundations*, vol. 26, no. 2, pp. 47-59, 1986.

[28] A. Asaoka and S. Ohtsuka, "Bearing capacity analysis of a normally consolidated clay foundation", *Soils and foundations*, vol. 27, no. 3, pp. 58-70, 1987.

[29] A. Asaoka, S. Ohtsuka, and M. Matsuo, "Coupling analyses of limiting equilibrium state for normally consolidated and lightly overconsolidated soils", *Soils and Foundations*, vol. 30, no. 3, pp. 109-123, 1990.

[30] S. Kobayashi, "Hybrid type rigid plastic finite element analysis for bearing capacity characteristics of surface uniform loading", *Soils and Foundations*, vol. 45, no. 2, pp. 17-27, 2005.

[31] T. Hoshina, "Rigid plastic stability analysis for slope including thin weak layer", *Japanese Geotechnical Journal*, vol. 6, no. 2, pp. 191-200, 2011.

[32] T. Hoshina, S. Ohtsuka, and K. Isobe, "Ultimate bearing capacity of ground by Rigid plastic finite element method taking account of stress dependent non-linear strength property", *Journal of Applied Mechanics*, vol. 6, no. 2, pp. I_327-I_336, 2012.

[33] N. L. Du, S. Ohtsuka, T. Hoshina, and K. Isobe, "Discussion on size effect of footing in ultimate bearing capacity of sandy soil using rigid plastic finite element method", *Soils and foundations*, vol. 56, no. 1, pp. 93-103, 2016.

[34] T. Iqbal, S. Ohtsuka, K. Isobe, Y. Fukumoto, and K. Kaneda, "Modified ultimate bearing capacity formula of strip footing on sandy soils considering strength non-linearity depending on stress level", *Soils and Foundations*, vol. 63, no. 3, 101325, 2023.

[35] P. N. Quang, P. N. Vinh, and H. P. Hoa, "Analyzing bearing capacity of a shallow foundation on cohesion-less soils under combined loads", *the 9th International Conference on Applying New Technology in Green Buildings (ATiGB)*, no. 9, pp. 32–37, 2024.